Title
3D Centrifugation-Enabled Priming of Synaptic Activation Promotes Primary T Cell Expansion

Journal
Advanced Therapeutics, 6(12)

ISSN
2366-3987

Authors
Jiang, Ruoyu
Chen, Yu-Hsi
Parajuli, Ritesh
et al.

Publication Date
2023-12-01

DOI
10.1002/adtp.202300224

ADVANCED THERAPEUTICS
www.advtherap.com

3D Centrifugation-Enabled Priming of Synaptic Activation Promotes Primary T Cell Expansion

*Ruoyu Jiang, Yu-Hsi Chen, Ritesh Parajuli, Anshu Agrawal, and Abraham P. Lee**

Autologous cell therapy depends on T lymphocyte expansion efficiency and is hindered by suboptimal interactions between T cell receptors (TCR) and peptide-MHC molecules. Various artificial antigen presenting cell systems that enhance these interactions are often labor-intensive, fabrication costly, highly variable, and potentially unscalable toward clinical setting. Here, 3D centrifugation-enabled priming of T cell immune-synapse junctions is performed to generate tight T cell–Dynabead aggregates at a rate 200-fold faster than that of conventional 24-h bulk shaking. Furthermore, by forming T cell–Dynabead aggregates in the starting culture, two- to sixfold greater T cell expansion is achieved over conventional T cell expansion for cancer patient-derived primary T cells while limiting over-activation. Creating 3D T cell–Dynabead aggregates as the "booster" material enables highly efficient polyclonal T cell expansion without the need for complex surface modification of artificial antigen-presenting cells (APCs). This method can be modularly adapted to existing T cell expansion processes for various applications, including adoptive cell therapies (ACTs).

1. Introduction

Rapid ex vivo T cell expansion is critical to produce a sufficient amount of functional T cells for T cell-based therapies. In treating melanoma and B cell acute lymphoblastic leukemia, T cell-based therapies, including tumor-infiltrating lymphocytes and chimeric antigen receptor (CAR) T cells, require at a minimum billions of T cells for successful clinical tumor detection and eradication.[1–4] Despite promising results obtained from recent clinical trials, ex vivo expansion of primary T cells has been challenging owing to the lengthy activation approaches.[5,6]

The first critical step for efficient T cell expansion is T cell activation. In the human body, the adaptive immune system depends highly on the clone-specific T cell receptors (TCRs) expressed on the surface of T cells to sense and detect foreign pathogens and malignant cellular changes.[7–9] T cell activation begins with TCRs recognizing antigenic peptides presented by the major histocompatibility complex (MHC) of antigen-presenting cells (APCs) and is completed by the presentation of co-stimulation cues.[10,11] Signal transduction to the cytoplasm is initiated upon such binding events.[12–14] During engagement events between peptide-MHC (pMHC) molecules and TCRs, actin cytoskeleton machinery alters the T cell membrane, restricts the interaction, and concentrates available peptide-MHC complexes by 100-fold to the center of the synapse.[15] Active cytoskeletal transport of TCRs exerts a wide range of forces (piconewton to nanonewton) that stabilize immunological synapses; T cell expansion proceeds with the addition of pro-survival cytokines.[16–18]

Approaches to facilitate ex vivo T cell expansion, by stabilizing the robustness of immunological synapses and artificial APCs (aAPCs), have been developed and extensively examined.[19–24] One of the most common commercial and clinically relevant approaches is based on Dynabeads functionalized with activating antibodies against CD3 (TCR stimulus) and CD28 (costimulatory cue).[25] Despite the success of polyclonal T cell expansion using these beads systems, the static and rigid bead surface does not fully represent how the surface of APC engages with T cells. To address this issue, various groups have created fluidic lipid membranes coated with ligands for TCRs and costimulatory molecules, mimicking natural engagement of APCs. Fluidic membranes are more effective than rigid spherical beads for creating immune-synapse clusters, generating significant T cell expansion.[26–29] The high aspect ratio of the bilayer lipid scaffold material (≈70 μm in length and ≈4.5 μm in diameter) or macroporosity of the 3D alginate structure, increases their interaction with T cells, resulting in greater proliferation and

R. Jiang, Y.-H. Chen, A. P. Lee
Biomedical Engineering
University of California
Irvine, CA 92697, USA
E-mail: aplee@uci.edu
R. Parajuli
Department of Medicine
Division of Hematology Oncology
University of California
Irvine, CA 92697, USA
A. Agrawal
Department of Medicine
Division of Basic and Clinical Immunology
University of California
Irvine, CA 92697, USA
A. P. Lee
Mechanical and Aerospace Engineering
University of California
Irvine, CA 92697, USA

The ORCID identification number(s) for the author(s) of this article can be found under https://doi.org/10.1002/adtp.202300224

DOI: 10.1002/adtp.202300224

expansion of human T cells than that of the smaller commercial Dynabeads (4.5 μm in diameter), thus providing better anti- tumor activity.[30–33] Exogenous force also contributes to enhanced T cell activation signals during culturing stages and doubles the expansion efficiency when cells and elastic droplet-based aAPCs are cultured under oscillatory shaking conditions.[17,34] Despite advances in the development of novel aAPC materials, current techniques focus on materials with diverse geometries and surface fluidity are costly, labor intensive and highly complex, thereby hampering their mass production for clinical use. Most aAPC systems are considered as "bottom-up" T cell activation methods designed for randomly distributed T cells and aAPC materials to engage and stabilize immune synapses, resulting in the formation of T cell–material clusters for clonal expansion.[35,36] During the initial interaction stage, the contact between pre-sedimented T cells and aAPC materials was randomly governed; this stochasticity places limitations on the initiation of T cell activation efficiencies. The lack of control during the initial contact and uneven bead-material distribution lead to suboptimal T cell expansion.[30,31,34,37–39]

We address this challenge by developing a top-down approach, as opposed to the conventional bottom-up T cell expansion strategy. This approach is based on a highly efficient high-throughput technique named 3D centrifugation-enabled priming of synaptic activation (3D CPS) that bypasses the stochastic nature of cell-aAPC contact and remodels the T cell activation microenvironment. We show that 3D CPS achieves a high contact ratio between human T cells and Dynabeads and forms cell–bead aggregates at high cell-bead density passing a time threshold. T cell activation interactions under 3D centrifugation is multifaceted, enabling multiple T cells to receive activation cues from multiple Dynabeads, which leads to highly concentrated immune-synapse junctions based on cytoskeleton mechanics.[16,39–42] By seeding T cell–material aggregates during the initial interaction stage, the cell–bead aggregates enhanced cell growth and served as centralized anchor sites to attract more T cells and Dynabeads, which grew around them. Finally, we applied 3D CPS to cancer patient derived T cells and promoted greater polyclonal activation and expansion than conventional static expansion methods. Taken together, the data suggest that 3D CPS does not require complex aAPC design and can easily be coupled with a diverse range of aAPC materials while limiting over-activation and readily used for the rapid expansion of functional T cells for adoptive cell transfer and other T cell-based cancer immunotherapies.

2. Results

2.1. 3D Centrifugation-Based Priming for T Cell Activation

The low diffusion speed of T cells and Dynabeads means that few contact events occur before sedimentation. We first hypothesized that an extremely high concentration would enable close contact. Interestingly, most of the interactions were between single T cells and single beads under 2D centrifugation on flat Countess cell counting slides (Invitrogen) at concentrations of 100 million particles per mL (T cell:Dynabead ratio, 1:1; Figure S1a, Supporting Information). Since there are multiple TCRs on single T cells, so 2D centrifugation limited physical contact areas of the TCRs to stimulating beads. The lack of physical contact sites of TCRs prompted us to design a 3D high concentration centrifugation environment, compacting the T cells and Dynabeads at the bottom of the V-shaped Eppendorf tube (**Figure 1**a). This ensures that the 3D interaction becomes multifaceted and involves single T cell contacting with multiple beads, maximizing the contact ratio. This system will also be compatible with a wide array of aAPC protocols. The force exerted by the TCR micro-clusters initiates T cell membrane protein reorganization, forming tight immune-synapse junctions (Figure 1a; Figure S1b, Supporting Information).

Once the cell–bead aggregates are formed in the high concentration environment, the TCR–anti-CD3-antibody bond must be cleaved. Although dense TCR clustering enhances T cell activation, overstimulation by the TCR stimulus can harm the T cells, causing cell exhaustion.[8,43] To address this issue, 3D centrifugation was restricted to a short incubation time for 6 min and then the cell–bead aggregates were transferred to 1 mL T cell culture medium for continued clonal expansion (Figure 1b). Since the cell–bead aggregates comprise multiple cells and multiple beads (4–10 T cells and Dynabeads), they are denser than single cells and thus sediment to the bottom of the well faster. This promotes closer interaction between the cells and beads at the bottom of the well (Figure S2, Supporting Information). Furthermore, the T cells expand following activation; this compounding effect increases the cell–bead skeleton size, thus attracting more suspended T cells and beads to participate in the interactions.

The impact of various dosing concentrations on the interaction behavior was investigated as a function of the cell–bead close-contact (μm) distance. The bulk activation processes were normally distributed, with 12% of the interactions exhibiting a close-contact cell–Dynabead distance peak at 30 μm; only 6% of the cells and beads interacted (**Figure 2**a). This distribution restricted the overall interaction rate, suggesting that very few cells were activated during the initial stage. The number of interactions increased as liquid was excluded, and the combined cell and bead concentration increased from 2 million to 100 million particles per mL (Figure 2a,b). The distribution peak eventually converged at 0 μm, with 50% of the cell population interacting with beads at 20 million particles per mL and 80% interacting with beads at 100 million particles per mL. In the 3D centrifugation environment (100 million particles per mL), the achieved interaction yield (contacted cells and beads) was 75.4 ± 3.0%, which is ≈17-fold higher than the 4.4 ± 1.3% achieved through bulk activation. This result ensures the transport of multiple T cell membrane cytoaggregates, thus initiating sufficient intracellular activation cascade (Figure 2c).

Based on the commercial protocol, the concentration threshold was set at 1 million T cells per mL of medium for culturing purposes.[30,34] To avoid overstimulation, the T cells were cultured with Dynabeads under extreme 3D centrifugation for 6 min and the cells and Dynabeads were reseeded by transferring them into 1 mL of T cell medium containing 30 U mL^{-1} IL-2 to continue the expansion process. We observed that non-stable immune-synapse junctions can be cleaved by manual pipetting, leaving only stable interacted cells and beads (14.2 ± 0.8%). In contrast, the conventional bulk process did not generate aggregates, and 45.0 ± 1.7% of the interacted cells formed tight cell–bead aggregates upon seeding (Figure 2d).

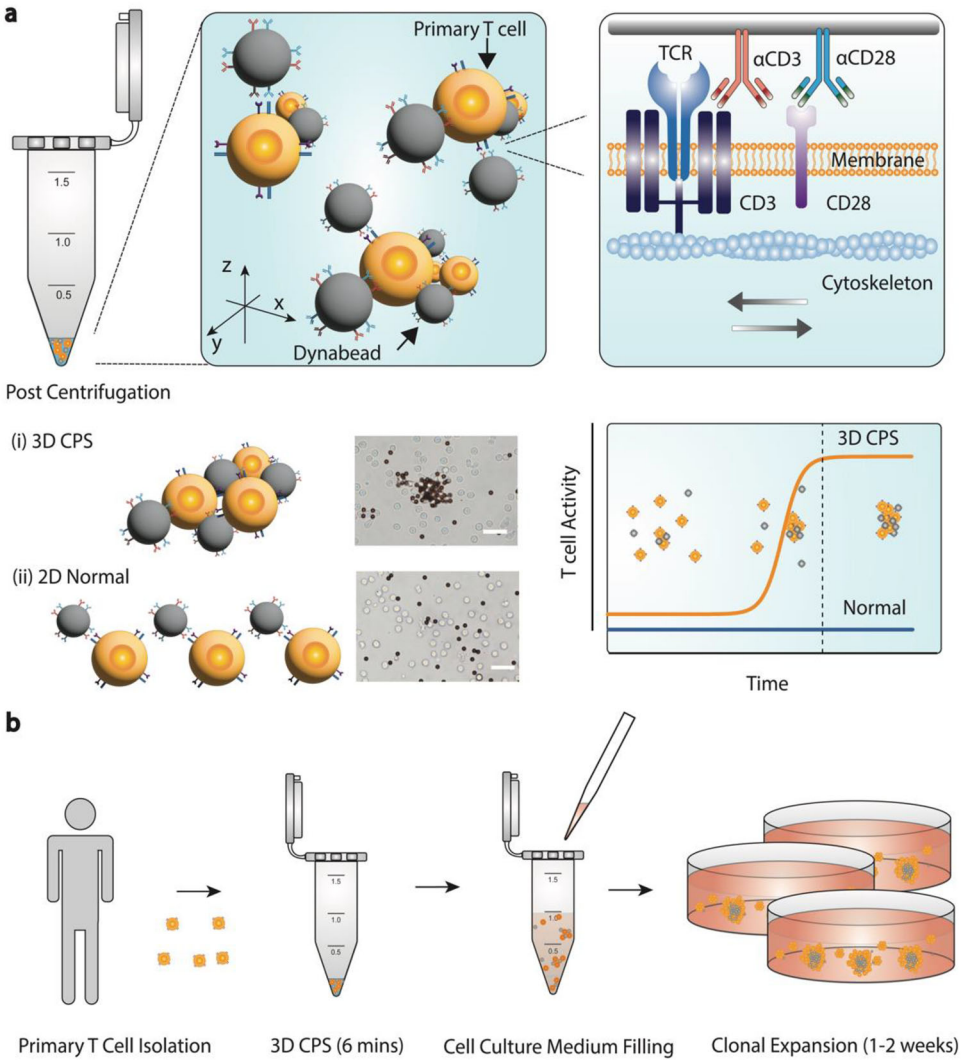

Figure 1. Workflow of 3D centrifugation-based priming. a) Human T-cell pellets are concentrated and confined with Dynabeads under V-shaped bottom. T cell–bead aggregates are formed from 3D centrifugation. (i) Representative images of T cell–Dynabeads aggregates from 3D centrifugation. Scale bar: 20 μm. (ii) Representative images of T cells and Dynabeads from 2D centrifugation. Scale bar: 20 μm. b. 3D CPS T cell expansion workflow.

To better understand how the 3D centrifugation approach affects T cell activation kinetics, the rate of T cell activation was quantified by measuring the fraction of interacted cells during the 24-h culturing process, at concentrations of 2 million and 5 million particles per mL. The interaction status was measured under 40× bright field magnification, imaged the growth process on a 24 well plate, and fitted the fraction of interaction states; the interaction rate constants (k) were 0.79 and 0.81 h^{-1} at 2 million particles per mL and 5 million particles per well, respectively (Figure 2E, **Figures 3,4**). The interacted fractions for these two concentrations remained at 72.7 ± 2.5% and 70.7 ± 2.7% at 24 h, suggesting that nearly a quarter of the seeded cells did not engage with the Dynabeads. At 20 million and 100 million per mL (3D CPS), the rate constants were 0.95 h^{-1} and 1.07 h^{-1}, respectively; at 24 h, their interacted fractions were 88.9 ± 6.9% and 87.6 ± 4.5%, respectively, suggesting that most of the cells engaged with the Dynabeads for activation (Figure 2e, Figures 3,4). This higher activation rate constant is primarily due to the greater number of cell–bead aggregates present in the starting materials; these aggregates serve as large scaffolds to enhance cell–bead adhesion.

2.2. Polyclonal Activation of Primary T Cells from Breast Cancer Patients

To assess the activation responses, the phenotype of the cultured human T cells was evaluated using 3D CPS at 100 million particles per mL conditions. The 3D centrifugation group consistently showed much larger cell–bead clusters than the bulk activation group, suggesting that the spatial arrangement of the cells and beads has a significant impact on the clustering behavior. Human T cells that were not incubated with Dynabeads exhibited no cluster formation (Figure 3a; Figure S5, Supporting Information). The 3D centrifugation approach achieved more centralized clusters, whereas the bulk approach generated scattered T cell clusters. The levels of activation marker CD25 were analyzed on

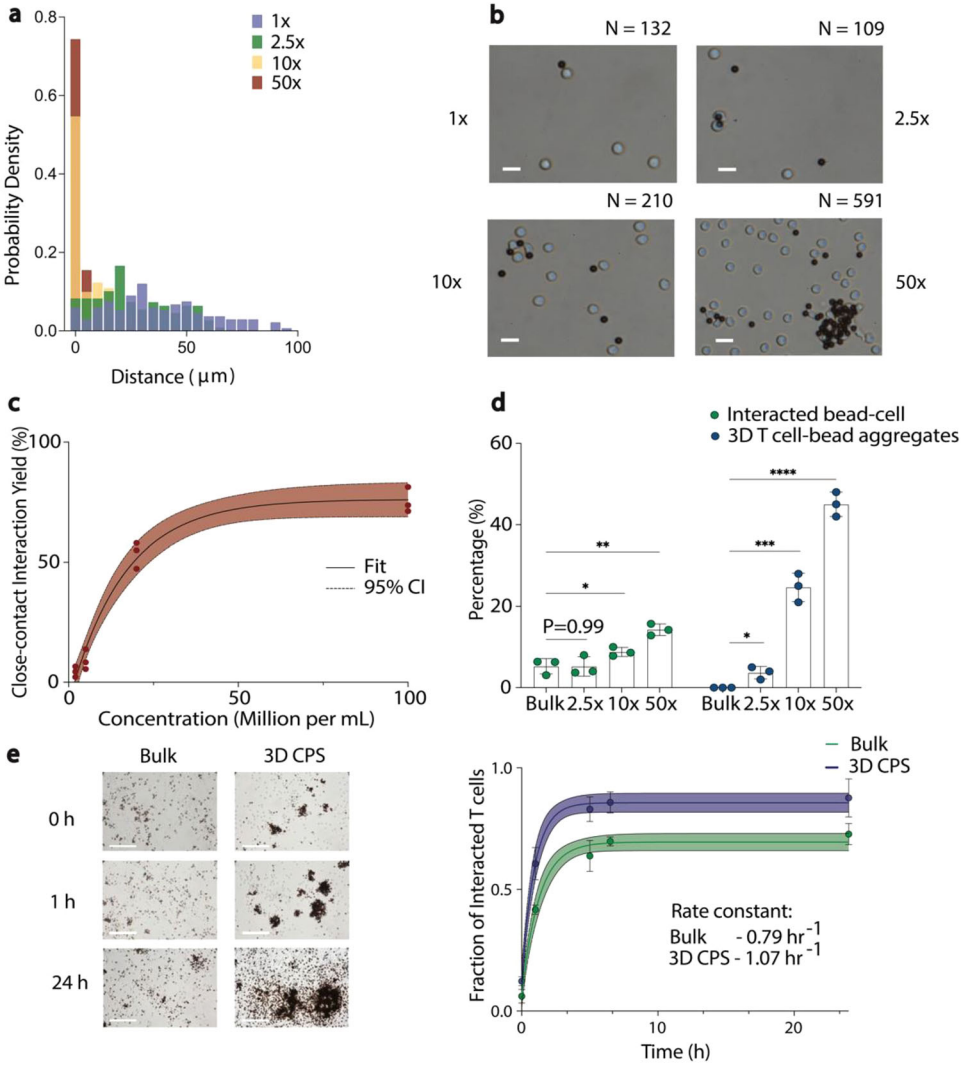

Figure 2. 3D CPS kinetics. a) Probability analysis of the close-contact distance (μm) under different 3D CPS conditions. b) Representative images for the bulk condition (2 million particles per mL), 2.5-fold concentrated cell solution (5 million particles per mL), tenfold concentrated solution (20 million particles per mL), and 50-fold concentrated cell solution (100 million particles per mL). N > 100 cells from three independent experiments. Scale bar: 15 μm. c) One-phase exponential function of 3D centrifugation concentration ($R^2 = 0.96$). d) Seeding process and percentages of cell–bead aggregates. e) Cell–bead skeleton growth over a 24 h period for bulk and 3D CPS. The fraction of joined cells and beads was used to fit the binding-rate constant. *P* values were determined using unpaired two-tailed *t*-tests. * $P < 0.05$, ** $P < 0.01$, *** $P < 0.001$, **** $P < 0.0001$. Bulk: Bulk activation. 3D CPS : 50x group.

day one to examine the activation efficiency, and CD69 expression was also analyzed to verify the activation signal (Figure 3b).

Under 3D centrifugation, the activated CD25-positive T cells fraction increased from 49.7 ± 7.4% to 77.4 ± 3.4% and the activated CD69-positive T cells fraction increased from 71.7 ± 1.7% to 90.8 ± 3.7% for cancer patient T cells using the flow cytometry gating strategy (Figure 3b; Figure S6, Supporting Information). CD25 expression was higher at the two higher particle centrifugation concentrations (20 million and 100 million particles per mL) than at the two lower concentrations (2 million and 5 million particles per mL; Figure 3d). To achieve the higher activation signal via the 3D centrifugation approach, a time threshold of 3–6 min was required (Figure 3d), consistent with the time needed to form the cell–bead aggregates. At times shorter than this 3D centrifugation incubation time, T cell activation was not enhanced.

2.3. Polyclonal Expansion of Primary T Cells from Breast Cancer Patients

The polyclonal expansion of primary T cells from breast cancer patients was investigated by culturing the cells for a two-week period and observing expansion on days 3, 7, and 14 using 3D CPS at 100 million particles per mL conditions. The higher activation signal achieved by the 3D centrifugation approach consistently generated larger T cell–bead clusters, while the bulk expansion

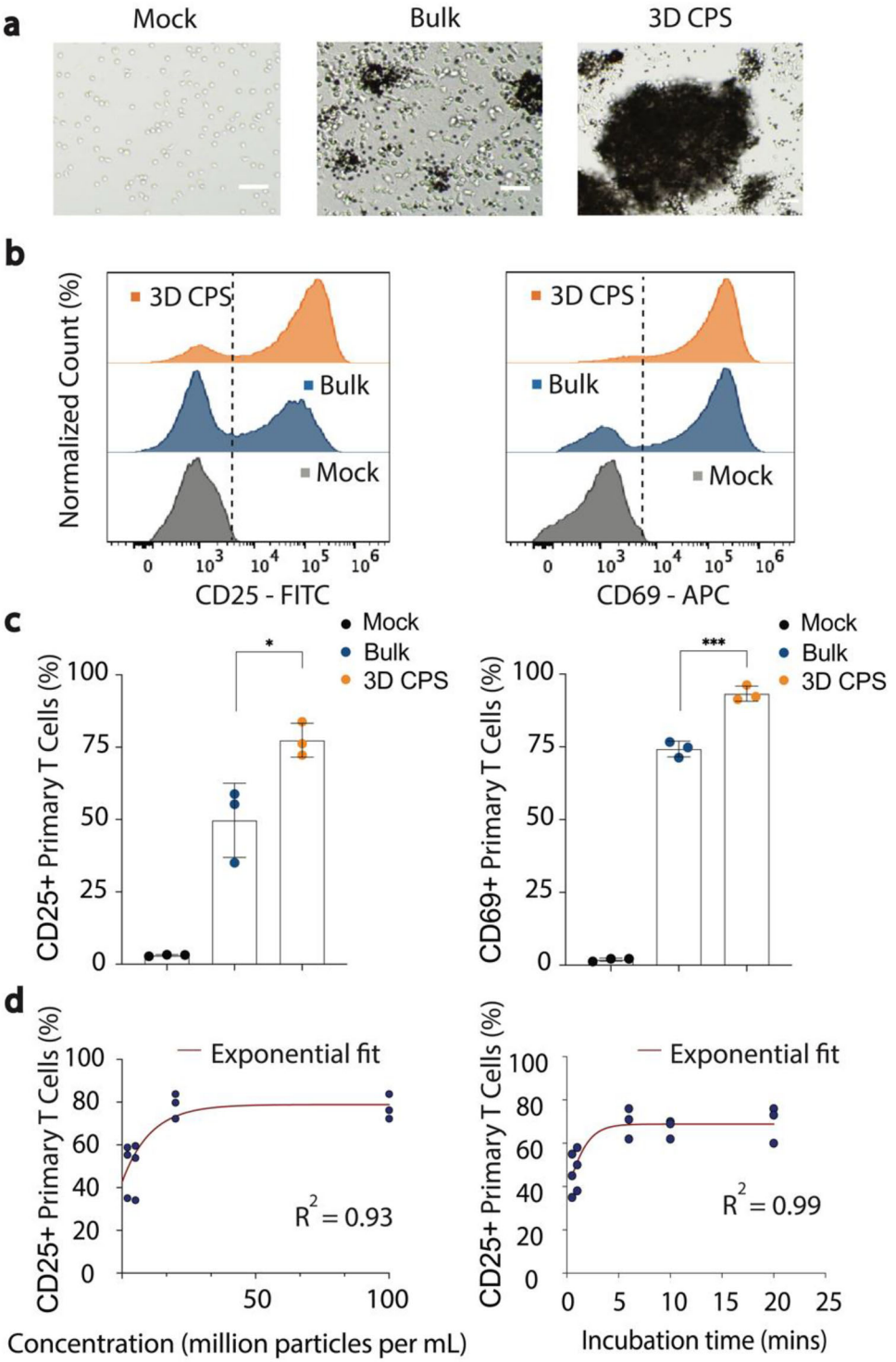

Figure 3. Polyclonal activation of patient-derived primary T cells. a) Representative bright field images of activation phenotypes for the mock (without Dynabeads), bulk (with Dynabeads), and 3D CPS group. Scale bar: 50 µm. b) Activation marker CD25 and CD69 analysis for bulk activation and 3D CPS groups. c) Percentage of activated human T cells (CD25- and CD69-positive T cells). *P* values were determined using unpaired two-tailed *t*-tests. * $P < 0.05$, ** $P < 0.01$, *** $P < 0.001$. d) Percentage of activated T cells as a function of centrifugation concentration and incubation time. Data in (c,d) represent mean ± s.e.m. of different donor samples and are representative of at least three independent experiments.

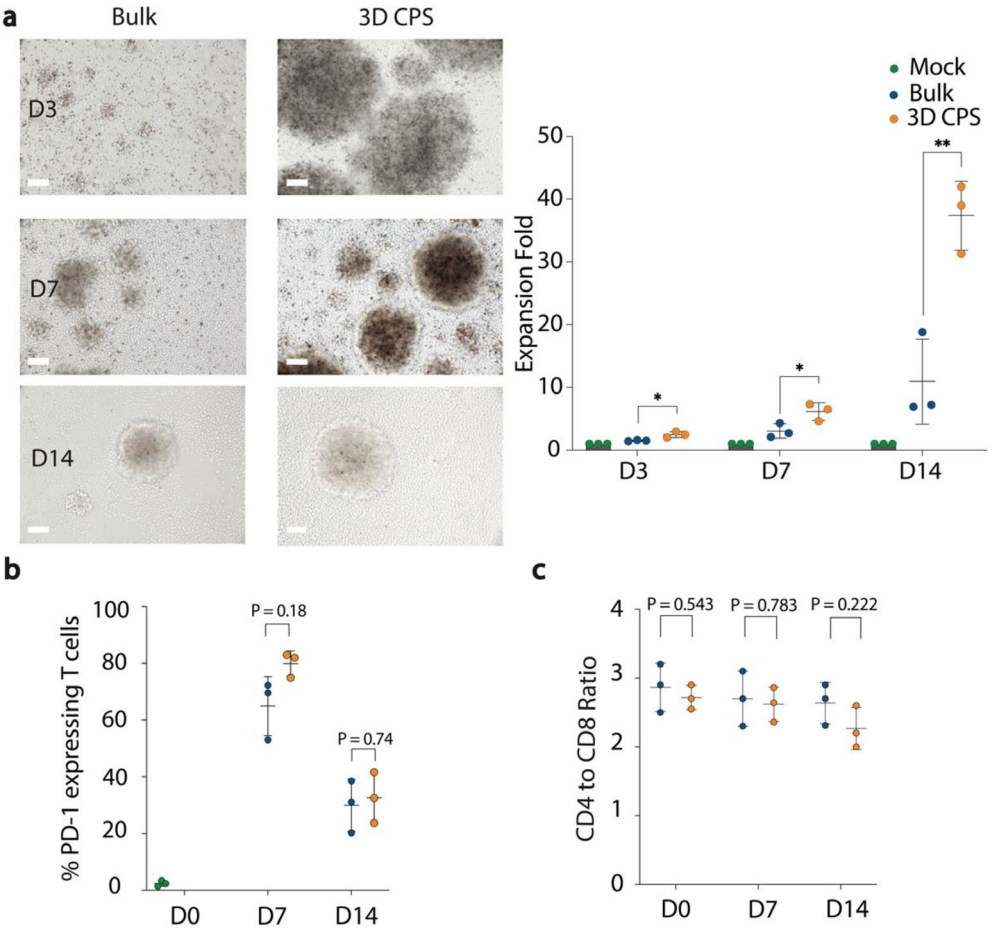

Figure 4. Polyclonal expansion of patient-derived primary T cells. a) Representative bright field images of expansion phenotypes and expansion fold for the bulk (with Dynabeads) and 3D CPS groups (100 million particles per mL) on days 3, 7, and 14. Scale bar: 50 µm. *P* values were determined using unpaired two-tailed *t*-tests. * $P < 0.05$, ** $P < 0.01$. b) Quantification of T cell PD-1 expression over the two weeks of clonal expansion. c) CD4:CD8 ratio among the $CD3^+$ cells on days 0 and 14 of T cell expansion. Data in (a–c) represent mean ± s.e.m. of different donor samples and are representative of at least three independent experiments.

group had much lower expansion rates and generated smaller T cell–bead clusters throughout the two-week period (Figure 4a; Figure S7, Supporting Information). This was supported by the much larger T cells observed for the 3D centrifugation group than for the bulk group; the size distributions showed larger cell diameters on day 3, 7, and 14 (Figure S8, Supporting Information).

Programmed cell death protein 1 (PD-1) expression was significantly higher on day 7 compared with day 0 in non-activated T cells, supported by the enhanced T cell activation, but showed similar expression between the 3D centrifugation group and the bulk expansion group, decreasing gradually to a similar level on day 14; this finding suggests that the 3D centrifugation approach did not induce severe cell exhaustion (Figure 4b; Figure S9a, Supporting Information). Cytotoxic T-lymphocyte-associated protein 4 (CTLA-4) expression was also measured at day 14, and both the bulk and 3D CPS groups presented a similar expression level (Figure S9b, Supporting Information). The CD4:CD8 ratio was ≈2:1 on days 7 and 14 for both bulk and 3D CPS groups, similar to the ratio prior to activation (Figure 4c, Figure S10, Supporting Information).

The proliferation of the expanded T cells was examined using flow cytometry to evaluate the expression of ki-67, an intracellular marker used to validate the proliferation index and expressed only in T cells undergoing cell mitosis cycles (G1, S, and G2 phases). Ki-67 expression increased significantly (by 71.53 ± 4.07%) under the 3D centrifugation approach, by 7.67 ± 0.73% under the bulk approach and by 0.04 ± 0.01% for the non-activated $CD3^+$ cells (**Figure 5**a, Figure S11, Supporting Information). Although higher ki-67 expression was associated with higher T cell proliferation, it did not directly reveal which cell division phases the T cells were undergoing.

Analysis of DNA mass via flow cytometry clearly revealed that the 3D centrifugation approach led to a higher proportion of proliferated T cells transitioning to the S and G2 phases, which are related to DNA replication and cell division, indicating rapid cell membrane and nucleus expansion. On the other hand, under the bulk approach, the proliferated T cells remained primarily at the G1 phase, which is related to cell growth (Figure 5b).

To further confirm this finding, Lonza electroporation was conducted on cultured primary T cells, which were transfected

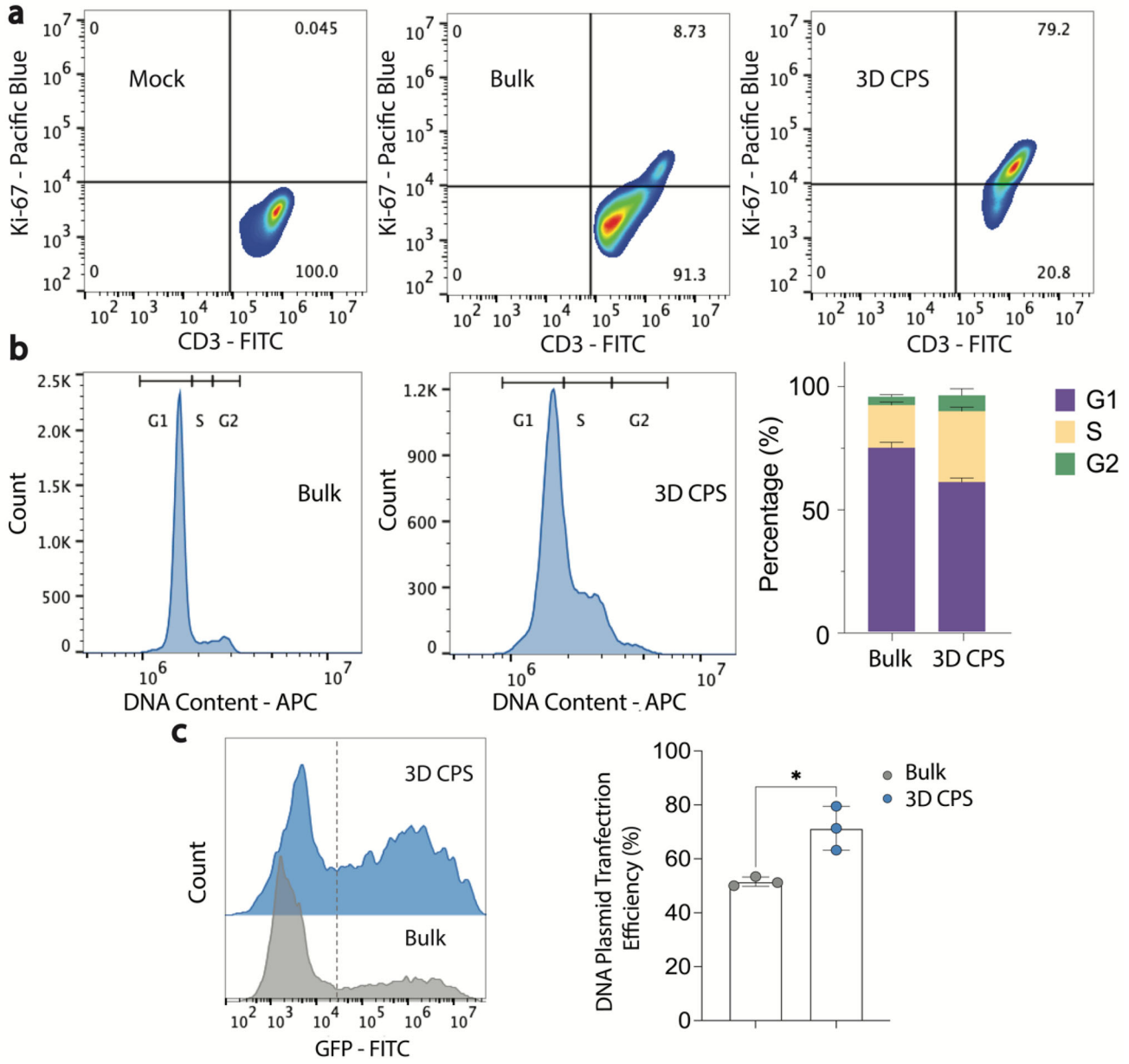

Figure 5. Proliferation of primary T cells. a) Intracellular ki-67 expression under the different expansion approaches. b) Cell cycle analysis on proliferated T cells. c) DNA plasmid transfection (eGFP) efficiency using the bulk and 3D CPS approaches. *P* values were determined using unpaired two-tailed *t*-tests. * $P < 0.05$. Data in (a–c) represent mean ± s.e.m. of different donor samples and are representative of at least three independent experiments.

with the green fluorescence protein (GFP) DNA plasmid. Deformation of the cell membrane and nucleus enhances plasmid uptake by the nucleus. Following electroporation, plasmid transfection efficiency was significantly higher in T cells with the 3D centrifugation approach than in those using the bulk approach protocol (Figure 5c, Figures 1,2).

3. Discussion

The 3D CPS method presented in this study has several advantages that make it suitable for adoption in primary T cell activation and expansion, as well as for use in cell biology, immunology, and the development of cell immunotherapy protocols. One key advantage is that the method is simple and can be easily adopted by general labs and clinics, as it uses commercially available standard Dynabeads. Additionally, the method generates densely packed T cell-bead complexes within minutes, which is a relatively rapid process compared to the 6–8 h required by current protocols. This makes the approach highly efficient for robust immune-synapse formation. The long formation time required in standard protocols is because they lack a deliberate architectural design to increase interactions during the initial culturing period before cell sedimentation. Current T cell expansion research focuses on engineering immune synapses after sedimen-

tation, and aAPC materials are frequently used, thus representing a more bottom-up approach (Figure S13, Supporting Information).

The 3D CPS method also has potential for ultra-high throughput, as each reaction can accommodate up to 10 million T cells while a centrifuge can accommodate up to 10 tubes with basic serial passaging. This allows for a substantially faster reaction times within small reaction volumes, making it possible to process large quantities of cells in a short amount of time. Another advantage of the 3D CPS method is that Dynabeads provide a static and rigid aAPC material that can be integrated with fluid-lipid bilayer membrane-aAPC materials to mimic how T cells engage naturally with APCs. This makes it possible to study T cell activation and expansion in a more physiologically relevant environment.

Polyclonal T cell expansion can be extended to antigen-specific T cell expansion by coupling the aAPC material with relevant tumor-antigen peptides or expanding CAR-T cells. In our study, we demonstrated the effectiveness of this method using breast cancer patient-derived T cells. This suggests that 3D CPS could also be useful in autologous monocyte-derived dendritic cell (moDC) therapy in clinics, to induce antigen-specific expansion of therapeutic T cells.[44–46] To enable the widespread application of the proposed approach in allogeneic cell therapy, we showed that 3D CPS can achieve healthy donor T cell polyclonal activation and enhances CD25-positive cells from 62.98 ± 2.97% to 78.33 ± 3.93% (Figure S14, Supporting Information). However, it is worth noting that the slightly lower signal elevation after 3D centrifugation in the cells from healthy donors may reflect intrinsic differences between primary T cells from cancer patients and healthy donors, which could be related to the antigen-exposure levels in the tumor microenvironment prior to T cell harvesting.[47,48]

The expansion of nuclear envelope during mitosis allows more effective entry of DNA into the nucleus and trigger physical enlargement, causing protrusions to extend from cellular membranes and the nucleus. Our results demonstrate that 3D CPS could be a valuable tool in CRISPR-based clinical trials targeting immunosuppressive factors like PD-1, endogenous TCR, and MHC-1, or CAR insertions in autologous and allogeneic T cells.[49–51] Our technique maximizes the surface density cues presented to T cells without inducing cellular exhaustion, which occurs when T cells are exposed to excessive levels of stimulatory molecules for extended periods. By forming high contact ratio aggregates as scaffolds before expansion, while maintaining the recommended culture concentration ratio (1:1 for Dynabeads:T cells), 3D CPS can induce extensive T cell expansion without inducing exhaustion, as reflected by similar levels of PD-1 and CTLA-4 expression in both bulk activation and 3D CPS groups.

3D CPS, inspired by a bottom-up/top-down development approach, represents a new paradigm for cell expansion. In the longer term, this method has critical advantages over conventional cell expansion approaches, not just in T cell-based therapy, but also in the rapidly growing area of antibody engineering. The critical step in 3D CPS that creates the T cell–bead aggregates can also be applied to T cell-dependent B cell stimulation. B cell expansion requires robust interactions between B cell receptors and other free soluble antigens, and between T helper cells and B cells via CD40 and MHC-II ligand binding. Rapid B cell clonal expansion forms B cell–T helper cell clusters; subsequent differentiation causes the maturation of B cells, which then produce antibodies such as IgG, IgA, or IgE.[52–56] 3D CPS therefore has the potential for large-scale antibody generation and related antibody selection in drug and vaccine development.

In conclusion, 3D CPS addresses a fundamental cell–material interaction challenge, by forming T cell–Dynabead aggregates via 3D centrifugation prior to culturing. By contrast, traditional T cell expansion relies on surface engineering of materials to regulate interactions. We demonstrated a method that is 200-fold faster over traditional bulk stimulation to enhance T cell–biomaterial interactions. Using standard Dynabeads, this method induced substantial T cell expansion, without inducing notable cell exhaustion.

Nonetheless, our method has potential limitations. For instance, the T cell–bead aggregates contain multiple T cells and multiple Dynabeads within highly concentrated scaffolds. Therefore, multiple Dynabeads may be able to engage with a single T cell, resulting in overstimulation of a small proportion of T cells. Our bulk protein analysis likely did not identify this overstimulation. In addition, although we focused primarily on polyclonal T cell activation and expansion, it is likely that the TCR binding and activation pathways depend on the T cell subtype; furthermore, the associated TCRs have various binding affinities toward an array of antigens.[57,58] To address this limitation, the T cell subtypes can first be sorted and the Dynabeads can be modified to incorporate various pathogenic peptides, prior to activation and expansion. Last, we were unable to measure the rate of membrane protrusion generated by the TCRs toward the Dynabeads under 3D centrifugation. High resolution methods to image and measure these forces may help in understanding the reported time and concentration thresholds.

In the future, it would be interesting to investigate whether soluble antibodies also induce skeleton formation under extreme 3D centrifugation. We plan to study how this method can be adapted for use with tumor-infiltrating lymphocytes and examine its anti-tumor activity via co-culture with cancer cells or solid tumors in a mouse model. This fundamental advance in immunology associated with the generation of stable immune-synapse junctions via 3D centrifugation within minutes could be applied to a broad range of aAPC material-based systems, thus offering a simple method of radically accelerating and enhancing T cell activation and expansion.

4. Experimental Section

Reagents and Cell Culture: Primary human T cells were cultured in T cell media supplemented with 30 U mL^{-1} recombinant human IL-2, unless otherwise stated. T cell culture medium was obtained from Gibco RPMI 1640 (Thermo Fisher Scientific, Waltham, MA) supplemented with 10% HI-FBS, 2 mM L-glutamine, 1 mM sodium pyruvate, 50 μM beta-mercaptoethanol, 0.1 mM non-essential amino acids, 1 mM sodium pyruvate, 10 mM HEPES, and 1% penicillin–streptomycin. Human CD3/CD28 T cell expansion Dynabeads were purchased from Thermo Fisher Scientific.

Primary T Cells Isolation: Primary human T cells were obtained from breast cancer patients who had previously consented to participate in a University of California, Irvine (UCI) IRB-approved clinical protocol permit-

ting blood collection (Clinical Trial UCI-17-43). Total T cells were purified using negative immunomagnetic kits (STEMCELL Technologies, Vancouver, Canada).

Primary T Cell Immunophenotyping: A step-by-step protocol was followed for the flow cytometry analysis for cell suspension samples (Biolegend, San Diego, CA). For the T cell activation experiments, the cell suspensions were stained concurrently with anti-CD25 and anti-CD69 antibodies. For the T cell expansion experiments, the cell suspensions were stained concurrently with anti-PD-1, anti-CD4, and anti-CD8 antibodies. The samples were then washed twice with PBS+ by centrifugation, and analyzed on a NovoCyte 3000 Flow Cytometer (ACEA Biosciences, San Diego, CA). Flow cytometry data were compensated using stained single-cell samples. Gates encompassing the positive and negative subpopulations within each compensation sample were used to calculate a compensation matrix in FlowJo (FlowJo, Ashland, OR).

Sample Preparation of 3D CPS: Human T cells were isolated from whole blood samples of patients with breast cancer using the negative immunomagnetic approach. One million human T cells were purified by removing the human plasma and sera, placed in T cell medium, and concentrated via serial gravity-based centrifugation at 350 × *g* for 5 min at 25 °C until reaching a final volume of 15 µL. One million Dynabeads (25 µL) were purified using Dynamaget (Thermo Fisher, USA) and concentrated fivefold into 5 µL bead volume by removing 20 µL of liquid. This sample was then manually transferred to incubate with the T cell pellets. The incubation lasted 6 min, and then the one million T cells and one million Dynabeads were transferred to 1 mL of cell culture medium in 24-well plates and then mixed thoroughly.

Polyclonal Primary T Cell Expansion Studies: T cells were enumerated with a hemocytometer (INCYTO, Republic of Korea) using Trypan blue exclusion. Expansion fold was calculated as follows: (number of total live cells at the respective time point)/(number of live cells seeded at the start of culture).

Intracellular ki-67 Staining: Patient-derived primary T cell were expanded with Dynabeads for 3 d. The cells were then washed twice with PBS and centrifuged at 350 ×*g* for 5 min. Then, 3 mL of cold 70% ethanol (−20 °C) was added to the cell pellets drop by drop, followed by gentle vortexing and incubation at −20 °C for 1 h. The cells were then washed twice with PBS and resuspended at 1×10^6 cells per mL. Then, 100 µL of cell suspension was mixed with Pacific Blue anti-human Ki-67 (Biolegend), followed by incubation at room temperature in the dark for 30 min. The cells were then washed and resuspended in PBS for flow cytometry.

Cell Cycle Analysis: Vybrant DyeCycle Ruby stain (Thermo Fisher Scientific) was equilibrated to room temperature. On day 3 of expansion, 0.5 mL of T cell suspension was prepared in T cell medium at 5×10^5 cells per mL. Vybrant DyeCycle Ruby stain (1 µL) was added to the cell suspension and mixed well at a final concentration of 5 µM, followed by incubation at 37 °C for 30 min in the dark. The cells were then analyzed without washing on a flow cytometer, using fluorescence excitation and emission maxima of 638 and 686 nm, respectively.

Imaging and Single-Cell Tracing: T cells and Dynabeads were imaged using an IX51 fluorescence microscope (Olympus, Japan) and an SLR camera at 40× magnification, on Invitrogen Countess cell counting slides (Thermo Fisher Scientific). The distance that the cells moved toward the beads was recorded and traced between the edges of the objects using ImageJ. Distances were then fitted to a cubic spline for extremely nonlinear relationships. Polar histogram analysis was performed using MATLAB.

Primary Human T Cell Electroporation: The 3 Kbp DNA plasmid encoding GFP (Lonza) was used to assess transfection efficiency. Electroporation was performed on the human T cells on day 3 of expansion, according to manufacturer's protocol, using cuvettes (100 µL), resulting in 1×10^6 cells per electroporation with 1 µg of the plasmid. The mixture was then gently transferred to T cell-medium and cultured at 37 °C in a humidified atmosphere. Flow cytometry was performed 24 h after electroporation, to assess green fluorescence expression.

Statistical Analysis: At least three cancer patient donors of all experiments were performed. Statistical analyses were conducted using Graphpad Prism v. 9, and data are presented as the mean ± standard deviation. The coefficient of determination (R^2) was used to indicate goodness of fit. Unless otherwise stated, groups were compared using two-tailed t-tests.

Supporting Information

Supporting Information is available from the Wiley Online Library or from the author.

Acknowledgements

The authors thank the training staff of the UCI Medical Center for their help in obtaining blood samples from consenting breast cancer patients. This work was supported by the National Science Foundation and the industrial members of the Center for Advanced Design and Manufacturing of Integrated Microfluidics (NSF I/UCRC award number IIP 1841509), American Cancer Society Institutional Research Grant (IRG-19-145-16) and the National Cancer Institute (NCI), 1R33CA267258-01A1) of the National Institutes of Health.

Conflict of Interest

The authors declare no conflict of interest.

Author Contributions

R. J. initiated the study, designed and implemented the experiments and analysis, and wrote the manuscript. Y. C. prepared samples, performed electroporation, and contributed to data analysis. R. P. prepared patient blood samples. A. A. provided guidance and contributed to data analysis. A. P. L. supervised the research and edited the manuscripts.

Data Availability Statement

The data that support the findings of this study are available from the corresponding author upon reasonable request.

Keywords

adoptive cell therapy (ACT), high-throughput mechanobiology, T cell activation, T cell expansion, T cell receptor (TCR)

Received: June 26, 2023
Revised: August 20, 2023
Published online: October 15, 2023

[1] M. E. Dudley, et al., *Science* **2002**, *298*, 850.
[2] S. L. Maude, N. Frey, P. A. Shaw, R. Aplenc, D. M. Barrett, N. J. Bunin, A. Chew, V. E. Gonzalez, Z. Zheng, S. F. Lacey, Y. D. Mahnke, J. J. Melenhorst, S. R. Rheingold, A. Shen, D. T. Teachey, B. L. Levine, C. H. June, D. L. Porter, S. A. Grupp, *N. Engl. J. Med.* **2014**, *371*, 1507.
[3] A. D. Fesnak, C. H. June, B. L. Levine, *Nat. Rev. Cancer* **2016**, *16*, 566.
[4] P. F. Robbins, S. H. Kassim, T. L. N. Tran, J. S. Crystal, R. A. Morgan, S. A. Feldman, J. C. Yang, M. E. Dudley, J. R. Wunderlich, R. M. Sherry, U. S. Kammula, M. S. Hughes, N. P. Restifo, M. Raffeld, C.-C. R. Lee, Y. F. Li, M. El-Gamil, S. A. Rosenberg, *Clin. Cancer Res.* **2015**, *21*, 1019.
[5] I. Mellman, G. Coukos, G. Dranoff, *Nature* **2011**, *480*, 480.

[6] Z. Wang, S. Ahmed, M. Labib, H. Wang, X. Hu, J. Wei, Y. Yao, J. Moffat, E. H. Sargent, S. O. Kelley, *Nat. Biomed. Eng.* **2022**, *6*, 108.
[7] S. A. Rosenberg, N. P. Restifo, *Science* **2015**, *348*, 62.
[8] L. V. Sibener, R. A. Fernandes, E. M. Kolawole, C. B. Carbone, F. Liu, D. Mcaffee, M. E. Birnbaum, X. Yang, L. F. Su, W. Yu, S. Dong, M. H. Gee, K. M. Jude, M. M. Davis, J. T. Groves, W. A. Goddard, J. R. Heath, B. D. Evavold, R. D. Vale, K. C. Garcia, *Cell* **2018**, *174*, 672.
[9] D. S. Jones, J. D. Nardozzi, K. L. Sackton, G. Ahmad, E. Christensen, L. Ringgaard, D.-K. Chang, D. E. Jaehger, J. V. Konakondla, M. Wiinberg, K. L. Stokes, A. Pratama, K. Sauer, T. L. Andresen, *Sci. Adv.* **2022**, *8*, abi8075.
[10] T. R. Mempel, S. E. Henrickson, U. H. Von Andrian, *Nature* **2004**, *427*, 154.
[11] J.-R. Hwang, Y. Byeon, D. Kim, S.-G. Park, *Exp. Mol. Med.* **2020**, *52*, 750.
[12] R. Evans, I. Patzak, L. Svensson, K. De Filippo, K. Jones, A. Mcdowall, N. Hogg, *J. Cell Sci.* **2009**, *122*, 215.
[13] F. Letourneur, R. D. Klausner, *Science* **1992**, *255*, 79.
[14] W. Zhang, J. Sloan-Lancaster, J. Kitchen, R. P. Trible, L. E. Samelson, *Cell* **1998**, *92*, 83.
[15] A. Grakoui, S. K. Bromley, C. Sumen, M. M. Davis, A. S. Shaw, P. M. Allen, M. L. Dustin, *Science* **1999**, *285*, 221.
[16] Y. Feng, et al., *Proc. Natl. Acad. Sci. USA* **2017**, *114*, E8204.
[17] K. H. Hu, M. J. Butte, *J. Cell Biol.* **2016**, *213*, 535.
[18] Y.-C. Li, B.-M. Chen, P.-C. Wu, T.-L. Cheng, L.-S. Kao, M.-H. Tao, A. Lieber, S. R. Roffler, *J. Immunol.* **2010**, *184*, 5959.
[19] A. N. Hasan, A. Selvakumar, R. J. O'Reilly, *Adv. Genet. Eng.* **2015**, *4*, 130.
[20] M. V. Maus, A. K. Thomas, D. G. B. Leonard, D. Allman, K. Addya, K. Schlienger, J. L. Riley, C. H. June, *Nat. Biotechnol.* **2002**, *20*, 143.
[21] K. Perica, J. G. Bieler, C. Schütz, J. C. Varela, J. Douglass, A. Skora, Y. L. Chiu, M. Oelke, K. Kinzler, S. Zhou, B. Vogelstein, J. P. Schneck, *ACS Nano* **2015**, *9*, 6861.
[22] T. M. D. Le, A.-R. Yoon, T. Thambi, C.-O. Yun, *Front. Immunol.* **2022**, *13*, 826876.
[23] S. Mandal, R. Hammink, J. Tel, Z. H. Eksteen-Akeroyd, A. E. Rowan, K. Blank, C. G. Figdor, *ACS Chem. Biol.* **2015**, *10*, 485.
[24] J. C. Sunshine, K. Perica, J. P. Schneck, J. J. Green, *Biomaterials* **2014**, *35*, 269.
[25] D. Hollyman, J. Stefanski, M. Przybylowski, S. Bartido, O. Borquez-Ojeda, C. Taylor, R. Yeh, V. Capacio, M. Olszewska, J. Hosey, M. Sadelain, R. J. Brentjens, I. Rivière, *J. Immunother.* **2009**, *32*, 169.
[26] T. M. Allen, P. R. Cullis, *Adv. Drug Delivery Rev.* **2013**, *65*, 36.
[27] R. Zappasodi, M. Di Nicola, C. Carlo-Stella, R. Mortarini, A. Molla, C. Vegetti, S. Albani, A. Anichini, A. M. Gianni, *Haematologica* **2008**, *93*, 1523.
[28] E. Ben-Akiva, R. A. Meyer, D. R. Wilson, J. J. Green, *Adv. Drug Delivery Rev.* **2017**, *114*, 102.
[29] Z. S. Dunn, J. Mac, P. Wang, *Biomaterials* **2019**, *217*, 119265.
[30] A. S. Cheung, D. K. Y. Zhang, S. T. Koshy, D. J. Mooney, *Nat. Biotechnol.* **2018**, *36*, 160.
[31] P. Agarwalla, E. A. Ogunnaike, S. Ahn, K. A. Froehlich, A. Jansson, F. S. Ligler, G. Dotti, Y. Brudno, *Nat. Biotechnol.* **2022**, *40*, 1250.
[32] J-Y. Chen, S. Agrawal, H.-P. Yi, D. Vallejo, A. Agrawal, A. P. Lee, *Adv. Healthcare Mater.* **2023**, *12*, 2203163.
[33] J. Van Der Weijden, L. E. Paulis, M. Verdoes, J. C. M. Van Hest, C. G. Figdor, *Chem. Sci.* **2014**, *5*, 3355.
[34] F. S. Majedi, M. M. Hasani-Sadrabadi, T. J. Thauland, S. Li, L.-S. Bouchard, M. J. Butte, *Nano Lett.* **2019**, *19*, 6945.
[35] A. Huber, F. Dammeijer, J. G. J. V. Aerts, H. Vroman, *Front. Immunol.* **2018**, *9*, 02804.
[36] M. Wieczorek, E. T. Abualrous, J. Sticht, M. Álvaro-Benito, S. Stolzenberg, F. Noé, C. Freund, *Front. Immunol.* **2017**, *8*, 00292.
[37] J. Guasch, M. Hoffmann, J. Diemer, H. Riahinezhad, S. Neubauer, H. Kessler, J. P. Spatz, *Nano Lett.* **2018**, *18*, 5899.
[38] B. R. Olden, C. R. Perez, A. L. Wilson, I. I. Cardle, Y.-S. Lin, B. Kaehr, J. A. Gustafson, M. C. Jensen, S. H. Pun, *Adv. Healthcare Mater.* **2019**, *8*, e1801188.
[39] M. H. W. Chin, M. D. A. Norman, E. Gentleman, M.-O. Coppens, R. M. Day, *ACS Appl. Mater. Interfaces* **2020**, *12*, 47355.
[40] E. Judokusumo, E. Tabdanov, S. Kumari, M. L. Dustin, L. C. Kam, *Biophys. J.* **2012**, *102*, L5.
[41] A. Isser, N. K. Livingston, J. P. Schneck, *Biomaterials* **2021**, *268*, 120584.
[42] B. Liu, W. Chen, B. D. Evavold, C. Zhu, *Cell* **2014**, *157*, 357.
[43] B. Alarcón, D. Mestre, N. Martínez-Martín, *Immunology* **2011**, *133*, 420.
[44] N. N. Hunder, H. Wallen, J. Cao, D. W. Hendricks, J. Z. Reilly, R. Rodmyre, A. Jungbluth, S. Gnjatic, J. A. Thompson, C. Yee, *N. Engl. J. Med.* **2008**, *358*, 2698.
[45] A. Mackensen, N. Meidenbauer, S. Vogl, M. Laumer, J. Berger, R. Andreesen, *J. Clin. Oncol.* **2006**, *24*, 5060.
[46] C. M. Rooney, C. A. Smith, C. Y. C. Ng, S. K. Loftin, J. W. Sixbey, Y. Gan, D.-K. Srivastava, L. C. Bowman, R. A. Krance, M. K. Brenner, H. E. Heslop, *Blood* **1998**, *92*, 1549.
[47] S. Y. Sheng, Y. Gu, C. G. Lu, J. Y. Zou, H. Hong, R. Wang, *Immunol. Res.* **2017**, *65*, 639.
[48] Y.-Y. Wang, N. Zhou, H.-S. Liu, X.-L. Gong, R. Zhu, X.-Y. Li, Z. Sun, X.-H. Zong, N.-N. Li, C.-T. Meng, C.-M. Bai, T.-S. Li, *Cancer Med.* **2020**, *9*, 5086.
[49] A. Katti, B. J. Diaz, C. M. Caragine, N. E. Sanjana, L. E. Dow, *Nat. Rev. Cancer* **2022**, *22*, 259.
[50] T. Haraguchi, T. Koujin, T. Shindo, Ş. Bilir, H. Osakada, K. Nishimura, Y. Hirano, H. Asakawa, C. Mori, S. Kobayashi, Y. Okada, Y. Chikashige, T. Fukagawa, S. Shibata, Y. Hiraoka, *Commun. Biol.* **2022**, *5*, 78.
[51] J. J. Ludtke, M. G. Sebestyén, J. A. Wolff, *Mol. Ther.* **2002**, *5*, 579.
[52] R. A. Manz, A. E. Hauser, F. Hiepe, A. Radbruch, *Annu. Rev. Immunol.* **2005**, *23*, 367.
[53] M. G. Mcheyzer-Williams, R. Ahmed, *Curr. Opin. Immunol.* **1999**, *11*, 172.
[54] M. Slifka, R. Ahmed, *Trends Microbiol.* **1996**, *4*, 394.
[55] M. K. Slifka, R. Antia, J. K. Whitmire, R. Ahmed, *Immunity* **1998**, *8*, 363.
[56] F. Franke, G. A. Kirchenbaum, S. Kuerten, P. V. Lehmann, *Cells* **2020**, *9*, 433.
[57] R. Glazier, J. M. Brockman, E. Bartle, A. L. Mattheyses, O. Destaing, K. Salaita, *Nat. Commun.* **2019**, *10*, 4507.
[58] V. P.-Y. Ma, Y. Hu, A. V. Kellner, J. M. Brockman, A. Velusamy, A. T. Blanchard, B. D. Evavold, R. Alon, K. Salaita, *Sci. Adv.* **2022**, *8*, abg4485.

